Iraqi Journal of Nanotechnology
synthesis and application
Journal Homepage : https://publications.srp-center.iq/index.php/ijn

Improvement of Morphological, Optical, and Electrical Properties of Nickel-Coated CdS Prepared by Thermal Deposition Method

Marwan Rasheed Abaas

Ministry of Education, Samarra Education Department, Samarra, Iraq
mastermarwan0@gmail.com

Keywords:
Thermal deposition;
CdSNi (NP);
Nano particle (NP).

Abstract

Pure and CdsNi (NP) were prepared by thermal deposition. The influence of the Ni doping ratio has studied these films' structural, morphological, optical, and electrical properties. Polycrystalline hexagonal (CdS and CdSNi) were shown to have [101] preferential orientation by XRD analysis. Images from the (FE-SEM) showed low-dimension NP formation, and the NP size was in the region of 15–25 nm. Optical analysis has shown that all the films are transparent. In the visible region, the transmittance ranges between 75% and 80%, were based on the concentration of the dopant. The film with a Ni ratio of 0.3 % showed a minimum resistivity of 6.14×10^5 Ω.cm at RT.

Introduction

Because of their widespread industrial application in nanoelectronic devices, nanostructured II-VI semiconductors have been studied extensively. Cadmium sulfide (CdS) is one of the most extensively studied materials among the II-VI compounds [1]. Because of their intriguing opto-electronic characteristics, II-VI semiconducting chalcogenide nanoparticles, particularly suldes and selenides, have been thoroughly studied [2]. (CdS) has a direct band gap of 2.42 eV at room temperature, making it a promising applicant for solar cells, green lasers, photoconductors, light-emitting diodes, and thin-film transistors [3]. Transition metal (TM) doped semiconductors, also known as diluted magnetic semiconductors (DMS), have attracted considerable scientific attention due to the potential applications they may have [4], such as a transparent semiconductor in other interesting applications [5], (LED) light emitting diodes [6], and spinotronic devices with diluted magnetic semiconductors [7]. To grow CdO thin films without doping or with doping, several chemical and physical methods, such as (S–G) [8], (SP) [9], (CBD) [10], (SILAR) [11], (RFS) [12], (MOCVD) [13], and (PLA) [14] were adopted. In this study, thermal deposition was used to improve the morphological, optical, and electrical properties of nickel-coated CdS(NP). With optimal production conditions, this method produces high quality thin films at a low cost.

Methods

1. Thermal deposition of thin films

A combination of 0.15 g CdS nanopowder and x g Ni nanopowder were bought to guarantee 99% purity (It was supplied by the Deutsche Solar AG company). (x = 0.1, 0.2, 0.3,0.4 to 0.5) was evaporated utilizing the technique of quasi-closed volume. Resistive molybdenum crucible on single crystal substrates with pre-cleaned and unheated glass was used. The deposition process was divided into 3 stages. In the first step the temperature of the source was maintained at 875 K for 8 min; in the second step the temperature was raised to 975 K and Kept for 4 minutes at this temperature. In the third stage, the temperature was elevated to 1120 K and held for 8 minutes at this temperature and the distance between the source and the substrate was 7 cm. The thin film was coded as CdS /substrate and CdS:x Ni / substrate (substrate= glass). The thickness of the film, measured by the interferometric process, was approximately 300 nm.

2. Characterization

Using a diffractometer "XPERT-PRO" device, the structure, crystallinity, and phase of the CdS and Ni-doped CdS(NP) were determined by using (XRD 6000 -SHIMADZU-Japan). Field Emission Scanning Electron Microscope device type (TESCAN MIRA3 FE-SEM) was used to visualize very small topographic information on the surface of a fractioned part or the entire of the sample. A UV-Visible 1800 Spectra Photometer was used to measure the band gap energy and the optical transmission of CdS and CdSNi. The electrical resistivity was measured in the dark and at room temperature.

Results and discussion

1. Determining crystal structure

For the XRD shown in Figure1, the Ni ratios of $CdS_{1-x}Ni_x$ (NP) were varied (x=0.1, 0.2, 0.3, 0.4% to 0.5%). It is evident from the shapes that the films in nature are polycrystalline, both peaks from the diffraction patterns 24.78, 26.47, 28.15, 36.59, 43.66,47.82 and 51.78 are typical of CdS undoped, indicating that integrating Ni into the films will not mean any shift in the CdS crystalline form. The interplanar d_{hkl} spacing values corresponding to the diffraction planes (1 00), (002), (1 0 1), (1 02), (11 0), (1 03) and (112) are contrasted with the CPDS card No: 64-3414 [15]. The measured dhkl values match the usual values, indicating that all deposited films (pure CdS and CdSNi) are hexagonal, with the crystals aligned in the path [101] parallel to the substrate [16]. Ni^{2+} ions were replaced with Cd^{2+} ions in CdS nanoparticles that had been doped with Ni^{2+}, and diffraction patterns showed a change in angle along major (101) planes. The CdS (NP) containing Ni ions are slightly shifted to the right, and this shift increases as the ratio of Ni ions in the (NP) increases. This means that the ratio of Ni doped CdS nanoparticles has an effect on the microstructure and crystal structure as shown in Figure 1. Figure 2 shows that Ni (0.1 %) doped CdS (NP) increased peak intensity (101) planes while Ni (0.2 %) doped CdS (NP) increased full width at half maxima (FWHM) while decreasing peak intensity, and Ni (0.5 percent) doped CdS (NP) increased FWHM while increasing peak intensity as shown in Figure 2. As a result of the substitution of the smaller ionic

radius Cd^{2+} ion (0.97) for the more massive Ni^{2+} ion (0.62), this process occurs. Figure 2b shows that the FWHM of CdS(NP) doped with Ni (0.3%) is reduced compared to other nickel percentages (0.1, 0.2 and 0.5 %), caused by the addition of Ni which is responsible for a small peak shift. In this case, the structural strain, is determined by [17]:

$$\varepsilon_s = -\Delta\,(\theta_{(101)})\ \cot g(\theta_{(101)}) \qquad (1)$$

The compressive stress that induces this structural strain can be measured with:

$$\sigma_{St} = (3\varepsilon_s)\ B \qquad (2)$$

B is the average CdS bulk module, that about 68.47 GPa [18]. As shown in Fig.3, the films' strain and stress initially decrease, pointing to the possibility that Ni^{2+} ions replace Cd^{2+} ions due to their smaller ionic radius (0.62 nm) than that of Cd^{2+} (0.97nm), before becoming nearly constant for Ni ratios of 0.2 to 0.4, implying that Ni^{2+} ions enter the lattice both substitutionally and interstitially.

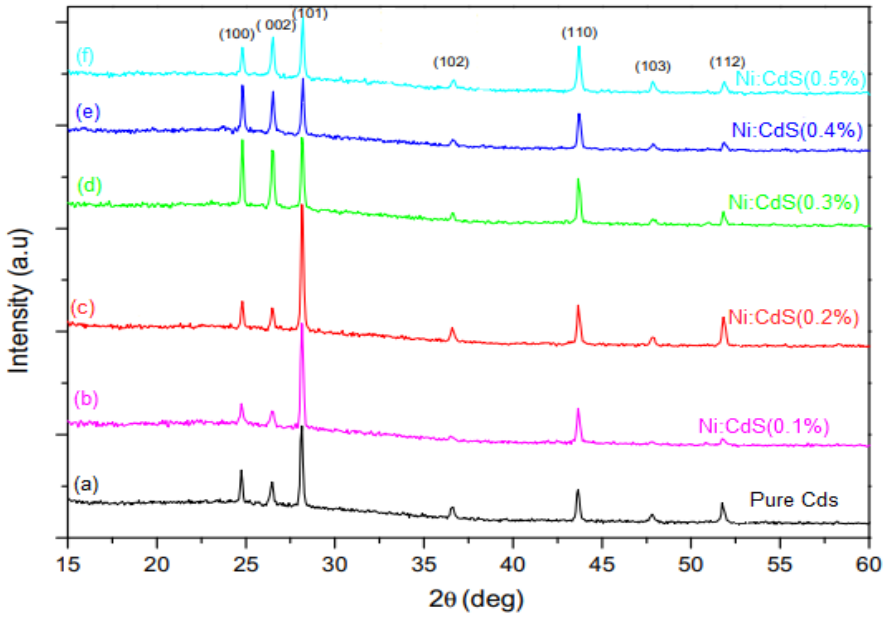

Figure 1 XRD diffraction diagrams of pure CdS and CdsNi : pure CdS, CdsNi (0.1%), (c) CdsNi (0.2%), CdsNi (0.3%), CdsNi (0.4%) and CdsNi (0.5%).

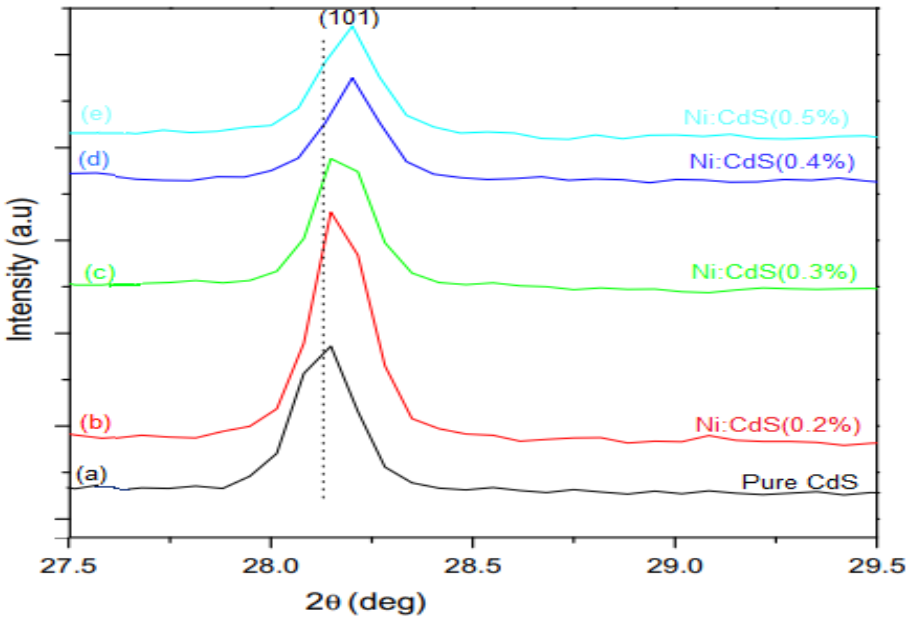

Figure 2 Variation peak position (101) of pure CdS and CdsNi : Pure CdS, CdsNi (0.2%), CdsNi (0.3%) ,CdsNi (0.4%) and CdsNi (0.5%)

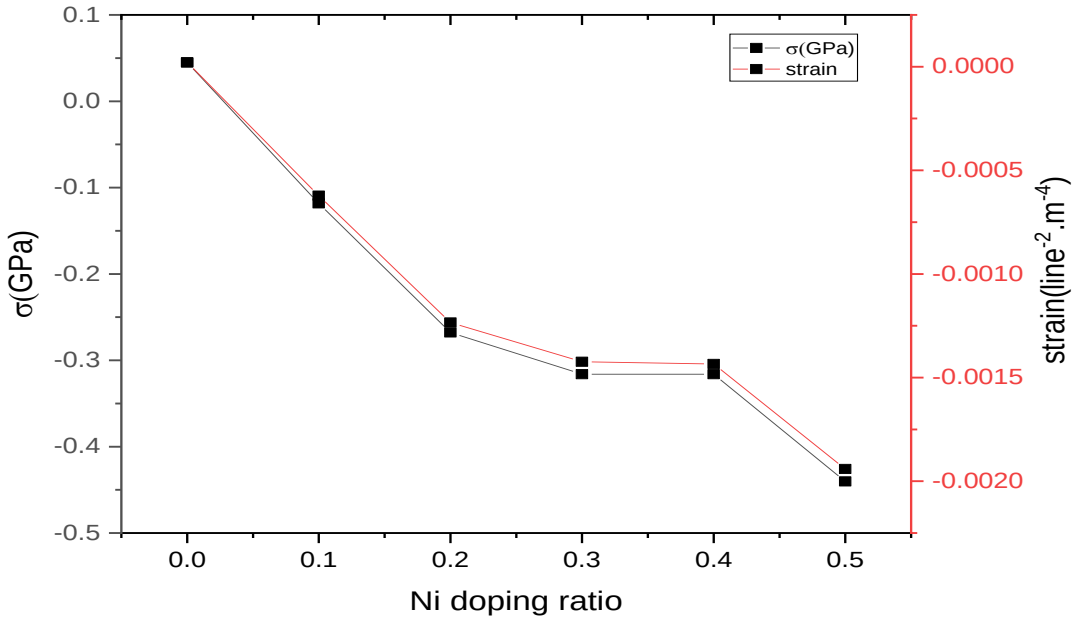

Figure 3 Structural stress and Ni doped ratio.

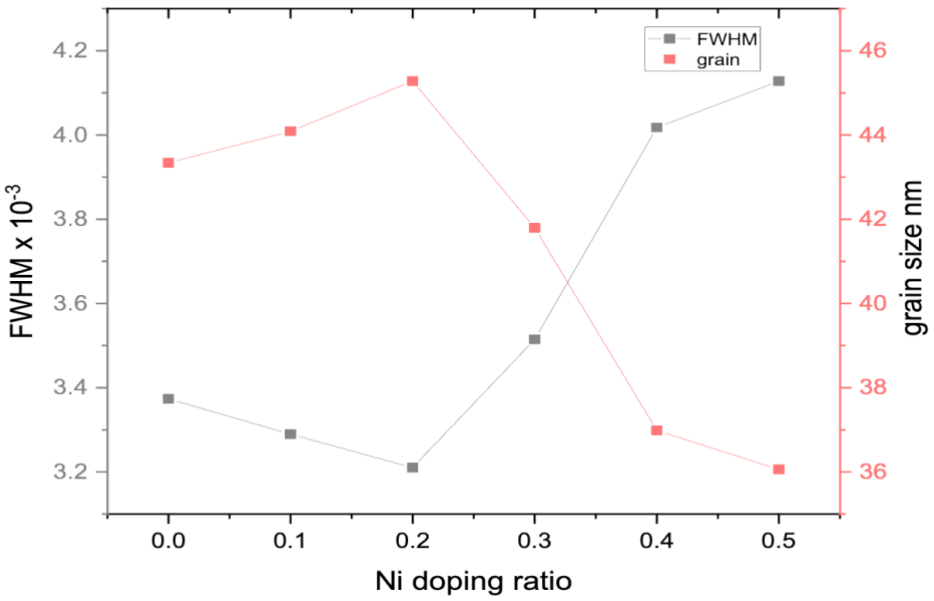

Figure 4 Ni doped ratio thin film average crystallite sizes and (FWHM).

Ni^{2+} ions in the lattice segregate inside grain boundaries when doped ratio approaches 0.4%. As shown in Figure 3, the compressive stress for CdSNi is usually between 0.1 and 0.44 GPa. However, the reduced stress value may produce a modest decrease in the lattice parameters, but not a structural change. CdSNi average grain size (D_{hkl}) is determined by XRD variations that use equation Scherrer [16].

$$D_{hkl} = 0.9\,\lambda / \beta_{hkl} \cos(\theta_{hkl}) \qquad (3)$$

When λ is the wavelength of the incident radiation (λ = 1,5406 Å), bhkl is the half-maximum width of the hkl line and hhkl is the Bragg diffraction angle. Figure 4 Shows the FWHM variance and the grain dependence Ni doping ratio. With a low Ni concentration (0.1%), grain size increases, and then decreases after Ni doping. Kim et al. [19] reported similar results for Ni-doped ZnO.

2. Surface morphology

The FE-SEM photos of the CdSNi nanoscale specimens are given in figure (5) (a – f). Both FE-SEM photos indicate low-dimension NP formation. The NP were extremely concentrated in pure state (Figure 5 (a)) and at small concentrations of Ni doping (Figure 4 (b) and (c)) and tended to be agglomerated with each other. For the pure, 0.1 % and 0.2 % CdSNi doped samples, the NP size was in the region of 15–25 nm. However, the NP tended to be separated (not much aggregated) at higher concentrations, and showed a spherical shape. Figure 5 d – f. The thickness of the Ni-doped NP increased with a rise in the concentration of Ni in CdS. The NP sizes for CdSNi were 23–30 nm in the range, which agrees with the estimated crystallite size using XRD data.

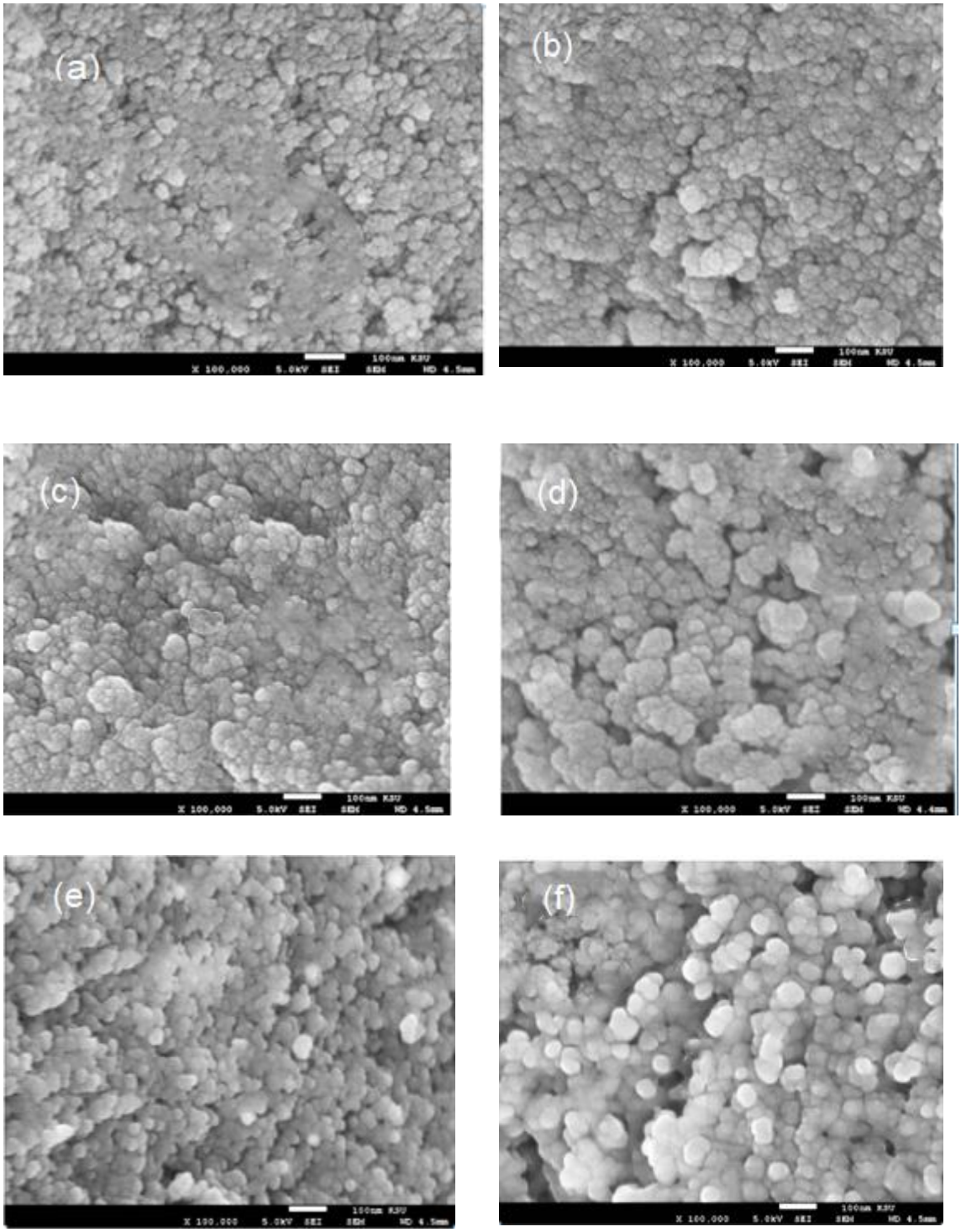

Figure 5 FE-SEM images of (a) pure and (b) 0.1%Ni, (c) 0.2%Ni, (d) 0.3%Ni, (e) 0.4%Ni, and (f) 0.5Ni% doped CdS NP.

3. Optical study

The variation of optical transmission with wavelength (k) in the range of 300 to 1500 nm is used to compute the optical properties of CdS(NP) such as transmittance, absorption coefficient, and band gap strength by equation :

$$T = (1-R)^2 \exp(-\alpha d) \qquad (4)$$

Transmittance (T), reflectance (R), calculated at 15% in the 300–1500 nm range, and film thickness (d). As can be observed, CdSNi samples are located comparatively with a strong clarity of approximately 75% in visible and near infrared areas, making it possible for solar cells to use it as a transparent window. In CdS films made in our lab using the CBD technique, we also observed a similar result [20]. In the VL and near IR regions, a CdS film doped with a concentration of 0.2 % has a transmission limit of around 70%. This can be clarified fairly by this film's fine crystallinity and stiochiometry, as identified through X-ray diffraction measurements. The transmission, however, decreases by 0.5 % Ni for the sample. This is due to a slight deterioration in the crystallinity of film as shown in Fig.6. Use the Tauc relationship, which is given by [21]:

$$(\alpha h\nu) = A\,(h\nu - Eg)^{n} \qquad (5)$$

For a semiconductor with a direct band gap like CdS, (hv) is the photon energy, (Eg) is the optical band difference, A is a constant, and n = 1/2. Fig. 7 shows the plot line (ahm) ^{2} versus photon energy that is used to measure the optical band gap of CdS(NP). The eV value of (Eg) has been found to range from 2.545 to 2.369 for films made at various Ni ratios. The change in energy levels owing to the exchange reaction may be referred to as it decreases. Chandramohan et al. showed similar results for Ni-doped thin CdS films obtained via implantation [3].

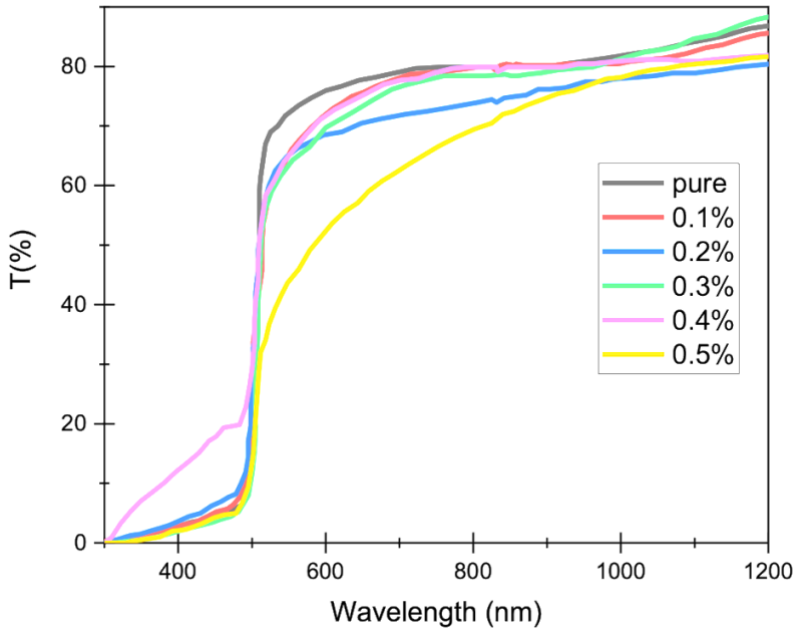

Figure 6 Transmittance spectrum of Ni-doped ratios

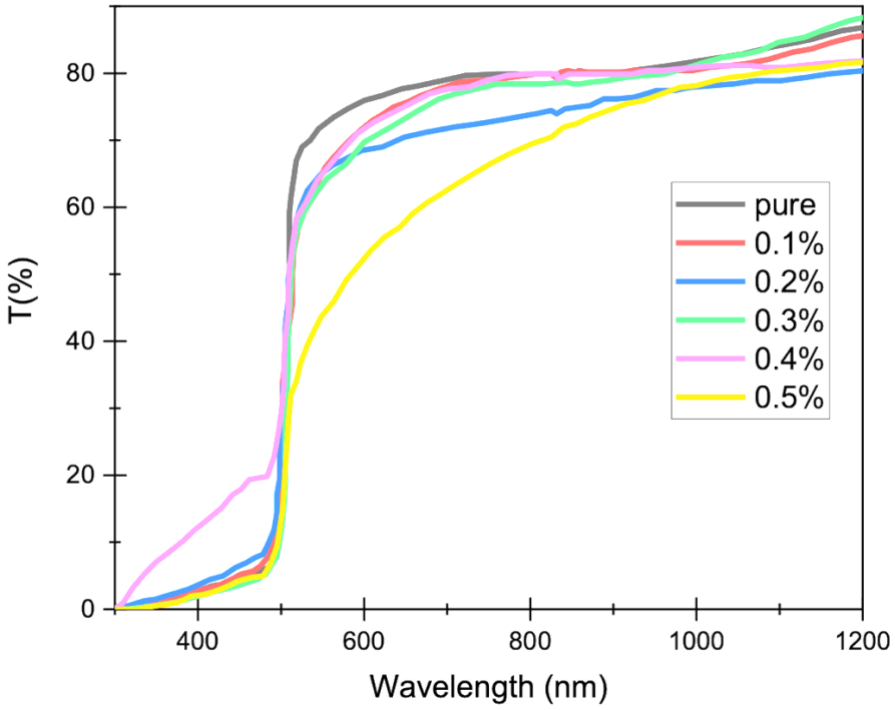

Figure 7 Transmittance spectrum of Ni-doped ratios

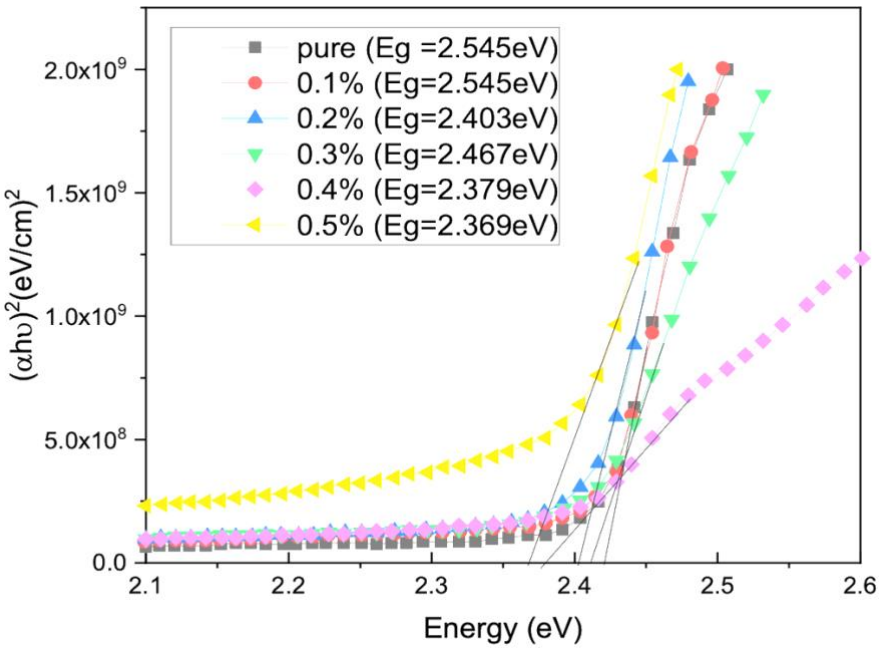

Figure 8 optical energy gap of Ni-doped ratios.

4. Electrical properties

For CdS(NP) with varying Ni ratios, the resistivity variation is shown in figure 8. Pure CdS films have a resistance of 5.5 x 10^6 cm. As the Ni ratio increases to 0.3 %, the resistivity increases to at least 6.14x10^5.cm. The decreased resistivity of CdSNi(NP) is explained by the substitution of Cd^{2+} ions by Ni^{2+} ions in the CdS lattice. However, large Ni doping ratios enhance film resistivity duo to CdO production in grain boundaries, as shown by XRD.

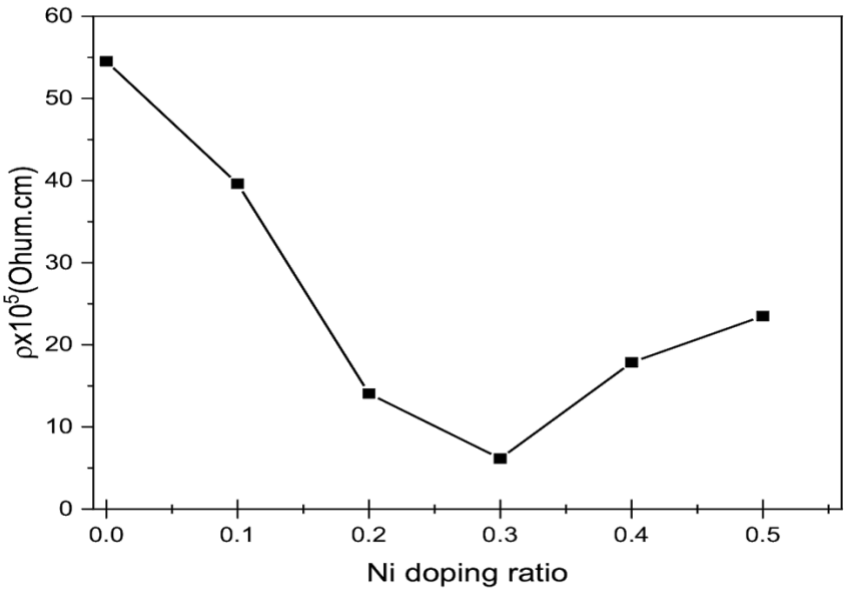

Fig. 8. Resistivity variation of Ni doping ratio

Conclusions

Deposited CdS(NP) pure and doped on amorphous glass substrates at room temperature. The Ni content affected the films' structural, optical, and electrical characteristic. The XRD indicates well crystallised hexagonal polycrystalline structure. X-ray diffraction revealed that when Ni content increases, film favoured orientation shifts from (10 1) to random. Optical measurements reveal that the band gap decreases as the Ni concentration increases. The produced films have a transmittance of around 70% in the VL and near-IR regions of the electromagnetic spectrum. As a result, the 0.3 % Ni had a minimum resistivity of $6.14x10^5$ cm. Because of its high transparency and low resistance, CdSNi(NP) used in solar cells and other optoelectronic devices as buffer layers.

References

[1] C. In-Hwan, C. hul-Hwan, Thin Solid Films 525 (2012) 132

[2] E. Bacaksiz, M. Tomakin, M. Altulbas, M. Parlak, T. Colagoklu, Phys. B: Condens. Mat. 403 (2008) 3740.

[3] S. Chandramodhan, T. Strache, S. Sarangi, R. Sathyamorthy, T. Som, Mater. Sci. Eng., B 171 (2010) 16.

[4] M.A. Mahdi, J.J. Hassan, S.S. Ng, Z. Hassan, N.N. Ahmad, Physica E 44 (2012) 1716.

[5] C. Hsu, D. Shen, Nanoscale Res. Lett. 7 (2012) 1.

[6] C. Shen, J. Chu, F. Qian, X. Zou, C. Zhong, K. Li, S. Jin, JMOp 59 (2012) 1199.

[7] M. Ren, C. Zhang, P. Li, X. Liu, JMMM 324 (2012) 2039.

[8] M. Thambidurai, S. Agilan, N. Muthukumarasamy, N. Murugan, R. Balasundaraprabhu, Int. J. Nanotechnol. Appl. 3 (2009) 29.

[9] A. Aschour, Turk. J. Phys. 27 (2003) 551.

[10] H. Khalaf, O. Oladeji, G. Chai, L. Chow, Thin Solid Films 516 (2008) 7306.

[11] M. Sasagawa, Y. Nosaka, J. Electroanal. Chem. 536 (2002) 141.

[12] H. Hemandez-Contreras, C. Mejia-Garcia, G. Contreras-Puente, Thin Solid Films 451 (2004) 203.

[13] S. Yoon, S. Lee, K. Seo, I. Shim, Bull. Korean Chem. Soc. 27 (2006) 2071.

[14] O. Vigil-Galan, J. Vida-Larramendi, A. Escamilla-Esquivel, G. Contreras-Puente,
F. Cruz-Gandarilla, G. Arriaga-Mejia, M. Chavarria-Castaneda, M. TufinoValasquez, Phys. Status Solidi A 203 (2006) 2018

[15] Standard JCPDS Data Card No. 892944, Physica 27 (1961) 337.

[16] A. Dakhel, Sol. Energy 83 (2009) 934.

[17] N. Benkhettou, D. Rached, B. Soudini, M. Driz, Phys. Status Solid 241 (2004) 101.

[18] L. Kadam, P. Patil, Mater. Chem. Phys. 68 (2001) 225.

[19] K. Kim, G. Kim, J. Woo, C. Kim, Surf. Coat. Technol. 202 (2008) 5650.

[20] F. Ouachtari, A. Rmili, B. Elidrissi, A. Bouaoud, H. Erguig, P. Elies, J. Mod. Phys. 2 (2011) 1073.

[21] J. Tauc, Amorphous and Liquid Semiconductors, Plenum Press, New York, 1974. p. 159.